ACCEPTED FOR PUBLICATION IN THE ASTROPHYSICAL JOURNAL LETTERS
Preprint typeset using LaTeX style emulateapj v. 26/01/00

THE IONIZED STELLAR WIND IN VELA X-1 DURING ECLIPSE

NORBERT. S. SCHULZ[1], CLAUDE. R. CANIZARES[1] JULIA. C. LEE[1] AND MASAO SAKO[2]

Accepted for publication in The Astrophysical Journal Letters

ABSTRACT

We present a first analysis of a high resolution X-ray spectrum of the ionized stellar wind of Vela X-1 during eclipse. The data were obtained with the High Energy Transmission Grating Spectrometer onboard the *Chandra* X-ray Observatory. The spectrum is resolved into emission lines with fluxes between 0.02 and 1.04×10^{-4} photons $cm^{-2}s^{-1}$. We identify lines from a variety of charge states, including fluorescence lines from cold material, a warm photoionized wind. We can exclude signatures from collisionally ionized plasmas. For the first time we identify fluorescence lines from L-shell ions from lower Z elements. We also detect radiative recombination continua from a kT = 10 eV (1.2×10^5 K) photoionized optically thin gas. The fluorescence line fluxes infer the existence of optically thick and clumped matter within or outside the warm photoionized plasma.

Subject headings: stars: early type — X-rays: stars — X-rays: neutron stars binaries: stellar winds — techniques: spectroscopic

1. INTRODUCTION

Massive early type stars show substantial mass loss through a strong wind. Matter is radially accelerated via momentum transfer from the stellar UV radiation field through absorption and scattering in resonance lines of abundant ions (Castor, Abott, and Klein 1975). In general the stellar wind itself is a source of X-rays, which form through reverse shocks generated by high density material in the wind (Lucy and White 1980, Owocki et al. 1988, Feldmeier et al. 1997). Typical observed X-ray luminosities range from a few times 10^{31} erg s^{-1} for early type B-stars to a few times 10^{32} erg s^{-1} for massive O-stars (Chlebowski et. al 1989, Berghöfer et al. 1995). Recent *Chandra* and *XMM-Newton* observations resolved the X-ray emission of several early type stars confirming the existence of collisionally ionized plasmas, but also suggested the possibility that alternative emission mechanisms for the observed X-ray emission need to be investigated. (Schulz et al. 2000, Kahn et al. 2001, Waldron and Cassinelli 2001).

The presence of a neutron star companion leads to a typical Bondi-Hoyle accretion flow (Bondi and Hoyle 1944), where a fraction of the stellar wind gets swept up by the neutron star, which generates a strong X-ray continuum. The X-ray luminosity of such a source is many orders of magnitudes larger than the one expected from shocks in the stellar wind, and X-rays from that source are reprocessed in the wind resulting in discrete emission lines (Stevens and Kallman 1990).

A prototype of such a system is the high-mass X-ray binary (HMXB) Vela X-1 (4U 0900-40). Its early type primary star HD 77581 is a massive B 0.5 Ib type supergiant (Brucato and Kristian 1972) with a mass and radius of 34 $R_\odot$ and 23 $M_\odot$ (from Nagase 1989), and an inferred mass loss rate of $> 10^{-7}$ $M_\odot$ yr^{-1} (Sato et al. 1986, Sako et al. 1999). The terminal wind velocity has been determined to be 1700 km s^{-1} (Dupree et al. 1980). The neutron star exhibits 282 s X-ray pulsations (Forman et al. 1973) and orbits the center of mass of the system at a distance of only about 0.6 stellar radii from the surface of the supergiant (a = 53.4 $R_\odot$) with a period of 8.96 days. This means that the neutron star is deeply embedded within the acceleration zone of the stellar wind.

The X-ray continuum of Vela X-1 has been studied extensively in X-rays. The general shape can be explained by a power law with a high energy cutoff typical for X-ray pulsars (White, Swank, and Holt 1983). Its average X-ray luminosity is $\sim 10^{36}$ erg s^{-1} , which is consistent with accretion from a stellar wind without Roche lobe overflow (Conti 1978).

In this paper we are primarily concerned with X-ray line emission from Vela X-1 during the middle of its eclipse. A first analysis of a moderate resolution X-ray line spectrum of Vela X-1 during eclipse was performed on a set observations with *ASCA* , which covered an entire eclipse transition from ingress to egress (Nagase et al. 1994). The observations revealed lines from He- and H-like ions species. It was suggested that the He-like transitions are formed by cascades following radiative recombination. Sako et al. 1999 identified recombination lines and radiative recombination continua produced by photoionization in an extended stellar wind. The deduced differential emission measure distribution was consistent with the wind model by Hatchett & McCray (1977). Sako et al. also indictated the existence of fluorescence lines from ion species of lower Z than Fe.

2. CHANDRA OBSERVATIONS AND DATA REDUCTION

Vela X-1 was observed with the HETGS on 2000 April 13th (09:57:52 UT) continuously for 28 ks. The HETGS carries 2 different types of transmission gratings, the Medium Energy Gratings (MEG) and the High Energy Gratings (HEG). It allows for high resolution spectroscopy between about 1 and 35 Å with a peak spectral resolution at 12 Å of $\lambda/\Delta\lambda \sim 1400$ and at 1.8 Å of $\lambda/\Delta\lambda \sim 180$ in 1st order HEG. The dispersed spectra were recorded with an array of 6 charged coupled devices (CCDs). We refer to the available Chandra X-ray Center (CXC) docments for more detailed descriptions of the spectroscopic instruments[3].

We recorded a total of 3200 events in the co-added 1st order

[1]Center for Space Research, Massachusetts Institute of Technology, Cambridge, MA 02139, nss, crc, jlee@space.mit.edu.
[2]Columbia Astrophysics Laboratory and Department of Physics, Columbia University, New York 10027, masao@astro.columbia.edu.
[3]http://asc.harvard.edu/udocs/docs/docs.html

MEG and 1700 events in the HEG after standard grade selection. The CXC provided aspect corrected event lists via standard pipeline processing. These data were reprocessed using the latest available data processing products. The wavelength scale has a zero point accuracy of 0.002 Å in MEG and 0.001 Å in HEG 1st order. The current status of the overall wavelength calibration is better than 0.05%. For the line analysis of the high resolution spectra we divide first by the instrument effective area and exposure, which is legitimate, because the spectral bin size is larger than the actual response of the instrument.

The image in the 0th order provides a source position as well as a medium resolution X-ray spectrum. The position of HD 77581 is well known to a precision of about 0.3 arcsec (Roeser et al. 1991). After correcting for a 2" aspect drift we find the position of the X-ray source to be within within 0.5" of this position. We also find no other X-ray sources within a radius of 30" around Vela X-1 with a flux above 1.2×10^{-15}erg cm^{-2} s^{-1} .

The CCD spectrum of that image also allows us to draw comparisons with previous *ASCA* observations, which are of similar spectral resolution, but cover a larger fraction of the eclipse. This CCD spectrum is only moderately piled up (7%) and can be used to determine qualitative characteristics of the observed emission as well as the total observed luminosity. The continuum model is the same as used by Sako et al. (1999), which consists of two absorbed power laws from the scattered component and a direct component with indices fixed to 1.7. The choice of this model is only motivated by the fact that we can draw comparisons with specifically the *ASCA* results. Since the spectrum shows significant line emission and we added several gaussian functions to fit the brighter lines observed in the *ASCA* spectrum (see table 2 in Sako et al. 1999).

In general we find good agreement with the *ASCA* results. The most striking difference is the column density of the direct component, which is twice as high and also indicates a much fainter direct component. This is a consequence of the fact that the *Chandra* observations exposure covers a smaller range in orbital phase around phase zero. We verfied this by re-analysing the *ASCA* data using the *Chandra* phase interval. From an X-ray flux of 0.88×10^{-11}erg cm^{-2} s^{-1} we then deduce 2.1×10^{33} erg s^{-1} for the luminosity (0.5-10 keV) assuming a distance of 1.9 kpc (Sadakane et al. 1985).

3. THE HETGS SPECTRA

The spectral continuum is well modeled in the zero order spectrum and we use it to subtract the continuum from the summed and background subtracted first order grating data. Figure 1 shows the residual spectrum between 3.1 and 12.5 Å .

3.1. *Fluorescence Emission*

The spectrum in Figure 1 shows a variety of fluorescent lines (green model) from Mg, Si, S, Ar, Ca, and Fe. The line properties, including possible identifications, are listed in Table 1. For identifications we use the adjusted calculations from House (1969). A few are also tabulated in Mewe (1994). The measured lines do not show significant velocity shifts or broadening and can be generally identified with near neutral charge states. For the elements Fe, Ca, and Ar we cannot distinguish between different charge states and here table 1 lists the most likely range based on the wavelengths given in House (1969). In the case of Mg, Si, and S we can identify various states, however for the lowest charge state we can again only identify a range of most likely ionization states.

For each detected line, we calculate an equivalent hydrogen column density required to produce the observed line fluxes using the method described in Sako et al. (1999). Fluorescent yields and photoionization cross sections are adopted from Kaastra and Mewe (1993) and Verner et al. (1996), respectively. Kaastra and Mewe (1993) predict an Fe Kβ/Kα flux ratio of ~ 0.13. We fix the width of the Kβ line to that of the Kα line and infer a ratio of 0.124 ± 0.095. Since this consistent with the theoretical value we assume that the iron line flux, and, hence the estimated column density, is not affected by resonant Auger destruction (Ross, Fabian, and Brandt 1996). Resonant Auger destruction occurs in regions, where line optical depths are significant. A fluorescent photon from the K-shell can be resonantely absorbed by ions that have vacancies in the L-shell. However, due to high autoionization yields in atoms of much lower Z than Fe, the L-shell ion will most likely Auger decay. In table 1 the quantity $Y_{\rm eff}$ denotes the fraction of the Fe Kα column density for each identified charge state of the other elements. For Fe K α we derive a column density of 3.3×10^{22} cm^{-2}. If the $Y_{\rm eff}$s are added up for each element we observe a correlation of the column density with Z, which could indicate the process of resonant Auger destruction at work. Such an interpretation was also given by Sako et al. (1999). However, for Si such an interpretation is problematic, since the Si VII and Si VIII lines appear exceptionally strong braking that correlation. In this respect the detection of fluorescent lines from L-shell ions suggests a somewhat modified explanation for the observed behavior.

TABLE 1
FLOURESCENT LINE ENERGIES AND FLUXES.

Ion	type[1]	λ^1_{exp} Å	λ_{meas} Å	Flux[2]	Y^3_{eff}
Fe	K β	1.756	1.748 ± 0.020	1.29 ± 0.88	0.950
	K α	1.937	1.937 ± 0.001	10.40 ± 1.08	1.000
	II - XI				
Ca	II-VII	3.359-3.352	3.356 ± 0.005	0.77 ± 0.04	1.015
Ar	VI-IX	4.186-4.178	4.184 ± 0.010	0.82 ± 0.04	0.460
S	IX	5.320	5.322 ± 0.018	0.43 ± 0.04	0.046
	IV-VIII	5.370-5.356	5.365 ± 0.018	1.26 ± 0.06	0.147
Si	IX	6.947	6.937 ± 0.004	0.33 ± 0.09	0.017
	VIII	7.007	7.008 ± 0.005	0.56 ± 0.14	0.036
	VII	7.063	7.059 ± 0.004	0.75 ± 0.14	0.054
	VI	7.117	7.117 ± 0.005	0.52 ± 0.14	0.042
	II-VI	7.126-7.122	7.124 ± 0.005	0.74 ± 0.13	0.048
Mg	V	9.814	9.827 ± 0.011	0.15 ± 0.07	0.0097
	II-IV	9.890-9.883	9.893 ± 0.008	0.17 ± 0.08	0.0115

[1] from House 1969
[2] in units of 10^{-5} photons cm^{-2}s^{-1}
[3] fraction of column density with respect to Fe K (uncertainties are $\sim$ 15%, in case of Mg 45%

3.2. *Radiative Recombination Continua (RRC)*

In photoionized plasmas, free electrons are captured by ions, which result in a continuous emission feature above the recombination edge (for a review, see Liedahl et al. 2001 and references therein). Since the plasma is overionized relative to the local electron temperature, the widths of these continua are narrow and appear as line-like features in the spectrum. RRCs from Ne X and Ne IX at 9.10 Å and 10.37 Å, respectively, are clearly observed. Although some of the features are rather

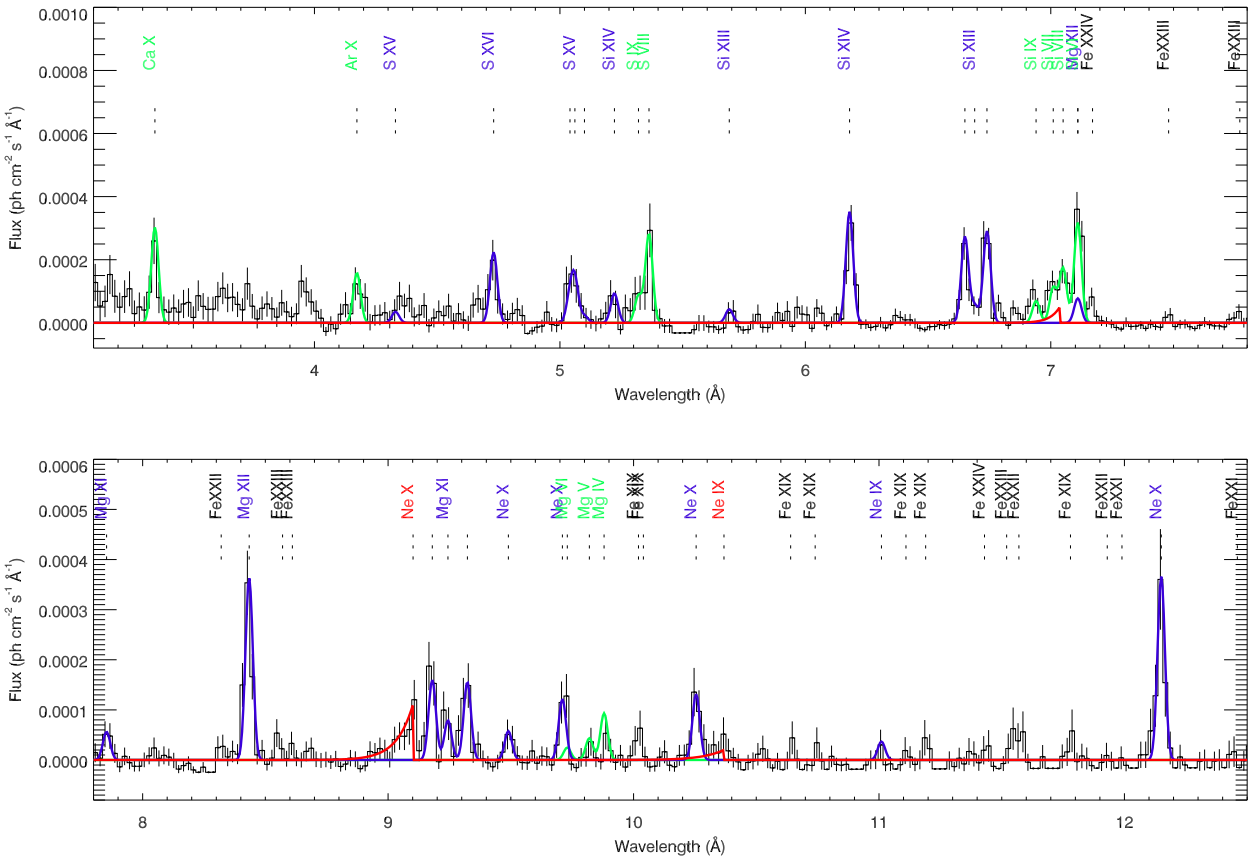

FIG. 1.— The residual HETGS spectrum in 0.02 Å bin with identified lines. Fluorescence lines are plotted in green. Highly ionized lines (blue) and RRC features (red) indicate an optically thin photoionized plasma.

weak, they are consistent with kT = $\sim 10 \pm 2$ eV (for Ne X) or a temperature of $T \sim 1.2 \times 10^5$ K. The Mg XI RRC is blended with the Si fluorescence lines, and a possible RRC of O VIII is observed at $\sim$ 14.25 Å. The detection of such narrow RRCs clearly indicates that there is a warm photoionized medium associated with the wind.

For Ne X at 12.13 Å and 9.10 Å , the measured Lyα/RRC flux ratio is $\sim 2.7 \pm 0.58$ after correcting for interstellar column density, and may be higher if there is additional absorption above the Galactic value. Liedahl and Paerels (1996) predict for the optically thin limit a ratio of 1.3 for a purely recombining plasma. Since this is inconsistent with the observed ratio, we assume that the assumption of a purely recombining plasma is not correct here. A more recent calculation by Kinkhabwala et al. (2001) also includes photoexitations in a more self-consistent manner and predicts a ratio of Lyα/RRC = 2.7 at kT = 10 eV which agrees well with our observations. The spectrum also exhibits very weak, but detectable amounts of line flux from Fe L ions. This is consistent with the prediction by Kallman et al. (1996) that recombination emission from K-shell ions dominates the spectrum in an overionized plasma.

3.3. *H- and He-like Lines*

The spectrum shown in Figure 2 also shows very strong emission lines (blue model) from H- and He-like S, Si, Mg, Ne, and possibly O. The measured line fluxes range between 0.2 and 3×10^{-5} photons cm^{-2} s^{-1}, and appear unresolved with no significant systematic line shifts. In the case of Ne X, four lines from the Lyman series are detected, with Lyα:β:γ:δ line ratios of 1.0:0.32:0.24:0.10 (with uncertainties of the order of 25%). The fluxes of higher lines in the Lyman series are larger than those expected from either a purely recombining plasma or a purely collisionally ionized plasma, and implies the presence of photoexcitation. This is consistent with the high Lyα/RRC flux ratio found in the previous section. For a photoionized plasma including the effects of photoexcitation self-consistently, the theoretical ratios for Ne X at kT = 10 eV are 1.0 : 0.35 : 0.16 : 0.08 at a column density of $N_{\rm NeX} = 3 \times 10^{17}$ cm^{-2} and a turbulent velocity of 300 km s^{-1} (Kinkhabwala et al. 2001). The Lyman series for Mg XII is difficult to assess since the Lyβ and γ appear blended.

The He-like lines of Si XIII and Mg XI are shown in Figure 2 (middle and right). In both cases the resonance and forbidden line fluxes have roughly equal strengths, which is not expected in a predominantly low density recombining plasma, but consistent with the fact that effects from photoexcitation have to be considered. It would therefore be incorrect to interprete these triplets using the calculations by Porquet and Dubau (2000), which in fact would predict a hot and dense collisional-dominated plasma. Such an interpretation would be in contrast with the results above, which indicate the presence of cool and warm photoionized media through the detection of narrow RRC and moderate line strength. Here Wojdowski et al. (2001) suggest that resonance scattering is the most probable probable process to enhance the resonance line in the He-like triplets.

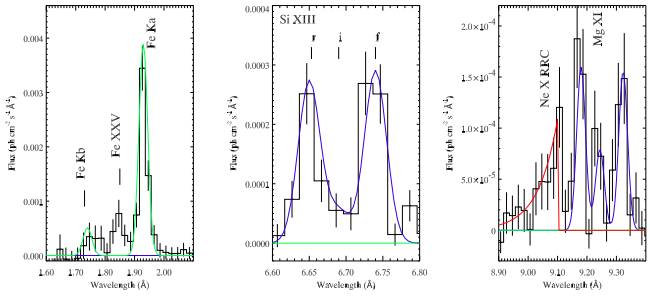

FIG. 2.— The Fe-K region (left) includes Fe K α and β line emission as well as a highly ionized Fe XXV line. The Si XIII He-like triplet (middle) shows a dominating resonance and forbidden line. The NE X RRC (right) appears at 9.10 Å below the Mg He-like triplet. Its fit indicates a temperature of ~ 10 eV.

We have yet to include contributions from the companion wind itself. In this case we have to consider collisionally ionized plasmas. Using the Astrophysical Plasma Emission Code (APEC, Smith et al. 2001), we can calculate line ratios between the Si XIII resonance line and Fe L lines at representative temperatures. Temperatures in O-stars range between $\sim 5 \times 10^6$ K (as measured in ζOri, (Waldron and Cassinelli 2001) and in an extreme case 5×10^7 K (as measured in θ Ori C, Schulz et al. 2000) from highly resolved X-ray lines. For now we assume that this is also a representative range of possible temperatures in the winds of B0.5 Ib supergiants. In the high temperature case we can exclude a significant contribution, because here Fe XXIV lines should dominate the spectrum, which we do not observe. Similarly, in the low temperature case Fe XVII lines should dominate the spectrum, which we do not observe either. For the intermediate range we estimate, under the assumption that the sporadic and weak detections of Fe L lines indeed reflect the existence of collisionally ionized emission, a contribution of a few percent at most.

4. CONCLUSIONS

The X-ray spectrum of Vela X-1 during eclipse shows a large variety of emission features including lines from H-like and He-like ions, RRCs, a population of very weak Fe L lines, and a number of fluorescence emission lines from mid-Z elements and iron indicating a complex structure of the X-ray emitting plasma.

From the fit of the shape of the Ne X RRC at 9.10 Å we deduce a temperature of 1.2×10^5 K for the plasma. Its flux ratio with the Ne X Lyman α line is consistent with an optically thin photoionized plasma. The spectrum shows clear evidence of photoexcitation processes, for which resonance scattering from the strong eclipsed X-ray continuum may be a likely source. More detailed calculations on this issue are required.

Fluorescence lines from various charge states were detected and partially identified. They include strong emission from M-shell ions, but also from various L-shell ions. Fluorescence yields are generally extremely low in mid-Z elements even at moderate optical depths. The correlation of the inferred column density with Z implies that autoionization dominates the fluorescence yields in these ions and the fluorescent plasma is not optically thin. If the fluorescent plasma coexists with an optically thin photoionized plasma or in a region outside the warm photoionized region, its has to be in the form of dense cool clumps. Both scenarios may be the case, which is not inconsistent with current stellar wind models. For example, Feldmeier (1995) pointed out that the wind can be devided into two distinct regions, an active inner one where shell to shell collisons occur and an outer, quiescent region with "old" material.

The detection of fluorescence from L-shell ions is still mysterious. Given the relative low fluorescent yields for these ions, resonant Auger destruction would have almost completely destroyed these lines. Further investigations of the possible mechanisms and physical conditions that prevent the lines from being destroyed are required.

The authors want to thank the MIT HETG team and the Chandra X-ray Center for their support, and Ali Kinkhabwala for providing results from calculations of photoionized plasmas in progress. This research is funded by contracts SV-61010 and NAS8-39073.

REFERENCES

Brucato R.J., and Kristian J., 1972, ApJ, 173, L105
Castor J.L., Abbott, D.C., and Klein, R.I, 1975, ApJ, 195, 157
Chlebowski T., Harnden F.R. jr., and Sciortino S., 1989, ApJ, 341, 427
Kahn S.M., Leutenegger M., Cottam J., Rauw G., Vreux J.M., den Boggende T., Mewe R., and Guedel M., 2001, A&A, 365, L312
Conti P., 1978, A&A, 63,225
Dupree A.K., et al., 1980, ApJ, 238, 969
Feldmeier, A., 1995, A&A, 299, 523
Feldmeier, A., Kudritzki, R.-P., Palsa, R., Pauldrach A. W. A., % Puls, J., A&A, 320, 899
Forman W., et al. 1973, ApJ, 182, L103
Gabriel A.H., and Jordan C., 1969, MNRAS, 145, 241
Hatchett S., and McCray R., 1977, ApJ, 211, 552
Kaastra J.S., and Mewe R., A&ASuppl., 97, 443
Kinkhabwala et al. 2001, in preparation
Liedahl D.A., Wojdowski P.S., Jimenez-Garate M.A., and Sako M., astro-ph/0105084
Lucy L.B., and White R.L., 1980, ApJ, 241, 300
Mewe R., 1994, SPEX version 1.0/Rev. 4.0
Morrison R., and McCammon D., 1983, ApJ, 278, 1082
Nagase F., 1989, PASJ, 41, 1
Nagase F., Zylstra G., Sonobe T., Kotani T., Inoue H., and Woo J., 1994, ApJ, 436, L1
Owocki S.P., Castor J.I., and Rybicki G.B., 1988, ApJ, 335, 914
Porquet D., and Dubau J., 2000, A&ASuppl., 143, 495
Roeser S., Bastian U., and Wiese K., 1993, A&ASuppl., 88, 277
Sadakane, K., Hirata, R., Jugaku, J., Kondo, Y., Matsuoka, M., Tanaka, Y., Hammerschlag-Hensberge, G., 1985, ApJ, 288, 284
Sato N., Hayakawa S., Nagase F., Masai K., Dotani T., Inoue H., Makino F., Makishima K., and Ohashi T, 1986, PASJ, 38, 547
Sako M., Liedahl D.A., Kahn S M., and Paerels F., 1999, ApJ, 525, 921
Schulz N.S., Canizares C.R., Huenemoerder D., and Lee J.C, 2000, ApJ, 545, 135
Smith, R.K., Brickhouse, N.S., Liedahl, D.A., & Raymond, J.C., 2001, ApJ, 556, L91
Stevens I.R., and Kallman T.R., ApJ, 365, 321
Verner D.A., Ferland G.J., Korista K.T., and Yakovlev D.G., 1996, ApJ, 465, 487
Waldron W.L., and Cassinelli J.P, 2001, ApJ, 548, 45
White N.E., Swank J.H., and Holt S.S., 1983, ApJ, 270,711
Wojdowski, P. S., Liedahl, D., A., Mauche, C. W., Sako, M, Paerels, F., & and Kahn, S.M, 2001, in *Two Years of Science with Chandra* , ed. M. Garcia, held at Washington DC, Sept. 5-7.